Journal of Alloys and Compounds 509S (2011) S540–S548

Contents lists available at ScienceDirect

Journal of Alloys and Compounds

journal homepage: www.elsevier.com/locate/jallcom

Effect of magnesium on the crystal structure and thermodynamics of the $La_{3-x}Mg_xNi_9$ hydrides

Roman V. Denys[a,b], Volodymyr A. Yartys[a,c,*]

[a] Institute for Energy Technology, Kjeller, NO 2027, Norway
[b] Karpenko Physico-Mechanical Institute, National Academy of Sciences of Ukraine, Lviv 79601, Ukraine
[c] Norwegian University of Science and Technology, Trondheim, NO 7491, Norway

ARTICLE INFO

Article history:
Received 4 November 2010
Received in revised form
18 November 2010
Accepted 25 November 2010
Available online 14 December 2010

Keywords:
Hydrogen storage
Metal hydride
Lanthanum
Magnesium
Nickel
Synchrotron X-ray diffraction
Neutron powder diffraction

ABSTRACT

The present work gives the data of systematic studies of the influence of magnesium on the crystal structure and hydrogenation behaviour of the *PuNi*$_3$-type $La_{1-x}Mg_xNi_3$ (x = 0–0.67) intermetallic alloys. Synchrotron X-ray diffraction studies revealed that substitution of La in $LaNi_3$ by Mg proceeds in an ordered way, only within the Laves type layers of the hybrid crystal structures build from the *MgZn*$_2$- and *CaCu*$_5$-type slabs. When completed, it leads to the formation of $LaMg_2Ni_9$ ($2MgNi_2 + LaNi_5$). Gradual increase of Mg content is accompanied by a linear decrease of the volumes of the unit cells. Interestingly, a substantial contraction takes place also for the Mg-free *CaCu*$_5$-type slabs. Hydrogen interaction with the $La_{1-x}Mg_xNi_3$ alloys was investigated by *in situ* synchrotron X-ray, neutron powder diffraction and pressure–composition–temperature studies. In the whole substitution range, $La_{1-x}Mg_xNi_3$ alloys form intermetallic hydrides with H/M ratio ranging from 0.77 to 1.16. Magnesium influences structural features of the hydrogenation process and determines various aspects of the hydrogen interaction with the $La_{1-x}Mg_xNi_3$ intermetallics causing: (a) more than 1000 times increase in equilibrium pressures of hydrogen absorption and desorption for the Mg-rich $LaMg_2Ni_9$ as compared to the Mg-poor $La_{2.3}Mg_{0.7}Ni_9$ and a substantial modification of the thermodynamics of the formation–decomposition of the hydrides; (b) an increase of the reversible hydrogen storage capacities following increase of Mg content in the $La_{1-x}Mg_xNi_3$ to ~1.5 wt.% H for La_2MgNi_9; (c) improvement of the resistance against hydrogen-induced amorphisation and disproportionation; (d) change of the mechanism of the hydrogenation from the *anisotropic* to *isotropic* one. Thus, optimisation of the magnesium content provides different possibilities in improving properties of the studies alloys as hydrogen storage and battery electrode materials.

1. Introduction

La–Mg–Ni intermetallic alloys are promising electrode materials for the advanced Ni-metal hydride batteries. Their electrochemical discharge capacity reaches 410 mAh/g, 30% superior compared to that of the $LaNi_5$-based electrodes [1].

Ternary La–Mg–Ni alloys relevant for electrochemical applications are related to the binary La–Ni intermetallic compounds of *PuNi*$_3$- and *Ce*$_2$*Ni*$_7$-types of crystal structures. $LaMg_2Ni_9$ intermetallic crystallizing in the trigonal *PuNi*$_3$-type structure was first reported by Kadir et al. [2,3]. Its crystal structure is a stacking of the $LaNi_5$ (Haucke *CaCu*$_5$ type) and $MgNi_2$ (Laves *MgZn*$_2$ type) slabs along the trigonal [0 0 1] axis. Initial study of hydrogen absorption–desorption properties of $LaMg_2Ni_9$ [4] showed its rather small hydrogen storage capacity of ~0.3 wt.%. This low value was explained by an inertness of the $MgNi_2$ slab to hydrogen absorption, similar to the properties of the individual $MgNi_2$ Laves type compound, which does not absorb hydrogen at conventional hydrogenation conditions [5].

Later research, however, showed that at lower Mg content, the related $La_{1+x}Mg_{2-x}Ni_9$ alloys containing mixed (La,Mg) Ni_2 slabs, show much higher values of the H storage capacities. Thus, these alloys exhibit superior characteristics in substituting the AB_5 alloys in the commercial Ni-MH batteries [6–9].

Liao et al. [7] found that in the ternary $La_xMg_{3-x}Ni_9$ alloys the *PuNi*$_3$ type is retained in the x range $1.0 < x < 2.0$, with the unit cell volumes linearly increasing with the La/Mg ratio. In parallel, it is observed an increase in the stability of the hydrides and an enhancement of the electrochemical discharge capacities, reaching 400 mA/g in maximum for the composition La_2MgNi_9.

Recent study of the phase diagram of the La–Mg–Ni system [10] showed that *PuNi*$_3$-type phase exists even in a broader concentration range leading to a continuous solid solubility between the $LaNi_3$ and $LaMg_2Ni_9$ stoichiometries.

* Corresponding author at: Institute for Energy Technology, Instituttveien 18, P.O. Box 40, NO 2027 Kjeller, Norway. Tel.: +47 63806453; fax: +47 63812905.
E-mail addresses: rdenys@ipm.lviv.ua (R.V. Denys), volodymyr.yartys@ife.no (V.A. Yartys).

0925-8388/$ – see front matter © 2010 Elsevier B.V. All rights reserved.
doi:10.1016/j.jallcom.2010.11.205

The electrochemical properties of $La_{1-x}Mg_xNi_3$ alloys were intensively studied and are reported in a series of publications. However, little is known about the structures of the corresponding hydrides and influence of the Mg/La substitution ratio on the structural and hydrogen gas sorption characteristics. Therefore, the main goal of the present work is in studies of the dependence of the Mg content in the $La_{1-x}Mg_xNi_3$ intermetallics on the crystal structures, hydrogen reversible storage capacities, and thermodynamics of the formation–decomposition of the hydrides. For convenience of comparison of our data with the previously performed research on the Mg substituted $LaNi_3$ alloys, we denote the chemical formula of the studied alloys as $La_{3-x}Mg_xNi_9$.

2. Experimental

Five $La_{3-x}Mg_xNi_9$ alloys, with $x = 0.5$, 0.7, 1.0, 1.5 and 2.0, were prepared by powder metallurgy route from the $La_{3-x}Ni_9$ alloy precursors and Mg powder (Alfa Aesar, 325 mesh, 99.8%). The $La_{3-x}Ni_9$ alloys were arc melted from the individual metals, La (99.98%) and Ni (99.9%), in a protective atmosphere of purified argon gas. As cast alloys were crushed into the powders and mixed with magnesium in suitable proportions. The powder mixtures ($m = 5$ g) were ball milled in a SPEX 8000D mill under argon for 8 h. After the milling process, the mixtures were annealed in argon atmosphere and then quenched into a mixture of ice and water. The annealing was performed in two steps; first, at 800 °C for 8 h, followed by a second step at 600 °C for 8 h. A small excess of Mg was introduced into the initial mixtures to compensate for its evaporation at high temperatures. Single phase $LaNi_3$ alloy was prepared by arc melting with subsequent annealing at 600 °C for 3 weeks and quenching to room temperature.

Initial phase-structural analysis was performed by X-ray powder diffraction using a Bruker D8 Advance diffractometer with Cu-K_α radiation. Accurate characterisation of the constituent compounds and determination of their crystal structures was performed using the data of synchrotron X-ray diffraction collected at a beam line BM01B of the Swiss Norwegian Beam Lines, ESRF, France using a monochromatic X-ray beam with $\lambda = 0.5009(1)$ Å. The experimental data were refined with Rietveld method using the Fullprof software [11].

Hydrogen absorption–desorption properties of the alloys were characterised using the Sievert's type gas system. The samples were activated in vacuum at 300 °C for 30 min, cooled to 20 °C and then charged with high purity hydrogen gas (purity 99.999%). Pressure–composition–temperature (PCT) dependences of hydrogen absorption and desorption were measured at temperatures from −40 to 70 °C and hydrogen pressures from 2×10^{-4} to 250 bar on the activated samples. Several complete hydrogen absorption–desorption cycles were performed prior to the PCT measurements to improve the kinetics of hydrogen exchange and to achieve maximum hydrogen storage capacities.

The *in situ* SR XRD data were collected at the beam lines BM01A ($\lambda = 0.7207$ Å) and BM01B ($\lambda = 0.5009$ Å), SNBL, ESRF. The measurements were performed using a setup designed for the SR studies of the chemical processes occurring in hydrogen gas or in vacuum. For the *in situ* SR XRD measurements the alloy powder was loaded into an open-ended 0.3 mm quartz capillary, which was then placed inside a sealed 0.5 mm capillary (wall thickness 0.01 mm). The 0.5 mm capillary was hermetically connected to the Sieverts' type gas system via a modified SS-Tee joint attached to a goniometer head. Averaging over the different orientations of the crystallites, resulting in the elimination of the preferred orientation effects in the collected diffraction data, is achieved by oscillating the setup around the axis of the capillary. Vacuum is created using a turbo molecular vacuum pump. Heating and cooling of the sample was performed at constant rates by a programmable air blower. The activation of the sample was performed by evacuating the sample cell at room temperature, filling it with hydrogen gas and heating to 120–150 °C to form a solid solution of hydrogen in the alloy. Then the sample was cooled down to form a saturated hydride. The desorption and absorption processes were performed at isobaric hydrogen pressure conditions, by heating or cooling the sample cell with a constant rate. By variation of the rate of changing the temperature, such method allows control over the hydrogenation/dehydrogenation rate. As a typical example of the collected experimental data, Fig. 1 shows changes in the SR XRD pattern during hydrogen absorption and desorption in the $La_{1.5}Mg_{1.5}Ni_9$–H_2 system.

In situ neutron diffraction studies of the $La_{3-x}Mg_xNi_9$-based deuterides were performed at the Spallation Neutron Source SINQ accommodated at Paul Scherrer Institute, Villigen, Switzerland, using a high resolution powder diffractometer HRPT in the high intensity mode ($\lambda = 1.494$ Å, 2θ range 4.05–164.9°, step 0.05°). The deuterides were synthesised in the stainless steel containers (wall thickness 0.2 mm, $d_{inner} = 6$ mm), which were connected to a Sieverts' type apparatus and used as the sample cells during the *in situ* NPD experiments. The samples were charged by deuterium gas (98% purity) at pressures from 5 to 25 bar, depending on the Mg composition.

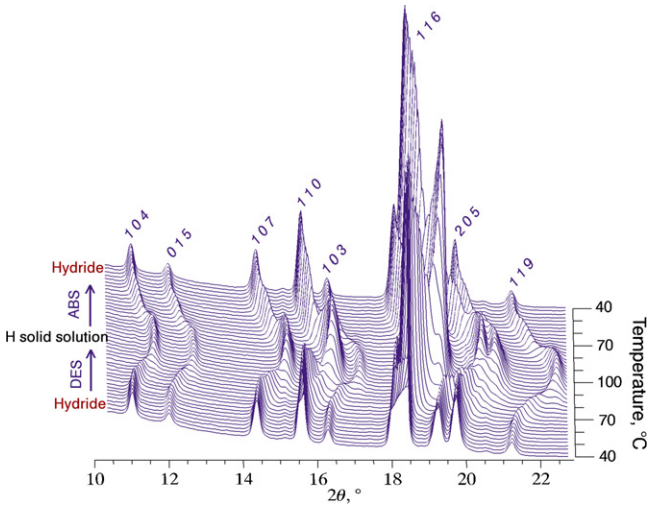

Fig. 1. *In situ* SR XRD pattern (BM01A; $\lambda = 0.7207$ Å) of hydrogen desorption and absorption in the $La_{1.5}Mg_{1.5}Ni_9$–H_2 system during heating and cooling at a constant rate (2 °C/min) under a constant hydrogen pressure of 23 bar. The data show a continuous phase transformation from the β-hydride $La_{1.5}Mg_{1.5}Ni_9H_{11}$ to the α-H solid solution in intermetallic alloy $La_{1.5}Mg_{1.5}Ni_9H_{\sim 1}$ proceeding on heating the sample from 40 to 100 °C. A complete reversibility of the formation of $La_{1.5}Mg_{1.5}Ni_9H_{11}$ was achieved during cooling of the sample from 100 to 40 °C.

3. Results and discussion

3.1. Effect of Mg substitutiton on the crystal structures of the $LaNi_{3-x}Mg_x$ intermetallics

Analysis of the XRD data showed formation of the trigonal $PuNi_3$ type intermetallics as the main constituents (>80%) for all studied $La_{3-x}Mg_xNi_9$ alloys ($0 \leq x \leq 2.0$). Above $x = 2.0$ the alloys become multiphase; further to $LaMg_2Ni_9$, they contain two secondary intermetallic phases, $MgNi_2$ and $LaNi_5$.

This is in agreement with previously reported formation of a continuous solid solution between the $LaNi_3$ and $LaMg_2Ni_9$ stoichiometries [10]. In addition, minor amounts of impurity phases, including $La_{1-x}Mg_xNi_2$, $La_{2-x}Mg_xNi_7$, $LaNi_5$ and $MgNi_2$, were identified in some alloys. Formation of these impurities depends on the magnesium content in the alloys and is in agreement with the diagram of phase equilibria in the La–Mg–Ni system [10].

For the single phase $LaNi_3$ intermetallic alloy, the refinements yielded the following crystallographic data: Space group $R\bar{3}m$; $a = 5.0842(2)$, $c = 25.106(1)$ Å; $V = 562.03(5)$ Å^3; La1 in 3*a*: 0, 0, 0; La2 in 6*c*: 0, 0, 0.1389(1); Ni1 in 3*b*: 0, 0, 1/2; Ni2 in 6*c*: 0, 0, 0.3328(3); Ni3 in 18*h*: 0.5003(7), 0.4997(7), 0.0802(2). The refined structure is in good agreement with the reference data [12].

The compositions of the studied $La_{3-x}Mg_xNi_9$ alloys and the corresponding crystal structure data obtained from the Rietveld refinements of high-resolution SR XRD data (see Fig. 2 as an example) are listed in Tables 1 and 2. Estimated standard deviations for the refined parameters were corrected to account for the serial correlation effects; the SCOR factors of 2.6–4.1 were applied and were calculated using the *Berar's* model [13] available in Fullprof. Crystallographic parameters for the $LaMg_2Ni_9$ and La_2MgNi_9 phases obtained in this work agree well with the published data [2,3] and [8], respectively. Because of the large differences in atomic radii ($r_{Mg} = 1.602$ Å *vs.* $r_{La} = 1.897$ Å), increase in the Mg/La ratio leads to a continuous decrease of both unit cell parameters, *a* and *c*. La substitution by Mg proceeds selectively, only inside the Laves-type slabs (6*c* site). The hybrid crystal structure of the $La_{3-x}Mg_xNi_9$ compounds is schematically shown in Fig. 3.

Interestingly, despite the selectivity of substitution leaves the $CaCu_5$ slab chemically unmodified, both $MgZn_2$ [(La,Mg)Ni_2] and

Table 1
Phase-structural composition and unit cell parameters of the $La_{3-x}Mg_xNi_9$ intermetallics from the Rietveld refinements of the SR XRD data (SNBL, BM01B, λ = 0.5009(1) Å).

Alloy	Phase	Structure type	Sp.gr.	Unit cell parameters (Å)		Content (wt.%)
				a	*c*	
$LaNi_3$	$LaNi_3$	*PuNi₃*	$R\bar{3}m$	5.0842(2)	25.106(1)	100
$La_{2.5}Mg_{0.5}Ni_9$	$La_{1-x}Mg_xNi_3$	*PuNi₃*	$R\bar{3}m$	5.06276(7)	24.6752(4)	86.6(1)
	$La_{1-x}Mg_xNi_2$	*MgCu₄Sn*	$F\bar{4}3m$	7.1754(3)	–	3.2(1)
	$La_{2-x}Mg_xNi_7$	*Ce₂Ni₇*	$P6_3/mmc$	5.0568(2)	24.500(1)	10.2(2)
$La_{2.3}Mg_{0.7}Ni_9$	$La_{1-x}Mg_xNi_3$	*PuNi₃*	$R\bar{3}m$	5.0488(2)	24.498(1)	80.5(2)
	$La_{1-x}Mg_xNi_2$	*MgCu₄Sn*	$F\bar{4}3m$	7.171(4)	–	8.4(4)
	$La_{2-x}Mg_xNi_7$	*Ce₂Ni₇*	$P6_3/mmc$	5.0477(4)	24.386(6)	11.1(5)
La_2MgNi_9	$La_{1-x}Mg_xNi_3$	*PuNi₃*	$R\bar{3}m$	5.0314(2)	24.302(1)	93.2(1)
	$La_{1-x}Mg_xNi_2$	*MgCu₄Sn*	$F\bar{4}3m$	7.1694(7)	–	6.8(3)
$La_{1.5}Mg_{1.5}Ni_9$	$La_{1-x}Mg_xNi_3$	*PuNi₃*	$R\bar{3}m$	4.9840(2)	24.006(1)	100
$LaMg_2Ni_9$	$La_{1-x}Mg_xNi_3$	*PuNi₃*	$R\bar{3}m$	4.94024(8)	23.8188(4)	80.2(7)
	$LaNi_5$	*CaCu₅*	*P6/mmm*	5.0180(1)	3.9777(2)	7.8(2)
	$MgNi_2$	*MgNi₂*	$P6_3/mmc$	4.8306(2)	15.836(1)	12.0(2)

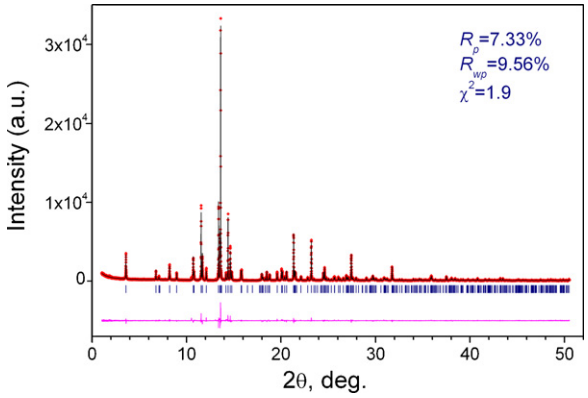

Fig. 2. Observed (+), calculated (upper line) and difference (lower line) SR XRD pattern of the single phase $La_{1.5}Mg_{1.5}Ni_9$ alloy (SNBL, BM01B, λ = 0.5009(1) Å).

CaCu₅ [$LaNi_5$] type slabs undergo a significant volume contraction, linearly depending upon the Mg/La ratio. Indeed, following the increase in the Mg content, a much more pronounced, up to 16%, volume contraction takes place for the (La,Mg)Ni_2 parts. Though the contraction is much smaller for the $LaNi_5$ layers, nevertheless, it reaches a rather significant value of 5%, if to consider that the chemical composition of these slabs remains unchanged. We note that both these values are comparable in absolute values with the volume effects caused by the formation of the metal hydrides (though these effects, obviously, are opposite in sign, being negative or positive). The observed relative changes in the unit cell volumes and the volumes of the *MgZn₂*- and *CaCu₅*- type slabs as compared with the corresponding structurally equivalent slabs of the $LaNi_3$ intermetallic structure are shown in Fig. 4.

3.2. Effect of Mg on the hydrogenation properties

$LaNi_3$ intermetallic compound interacts with hydrogen via two different mechanisms, depending on the hydrogen pressure–temperature conditions applied.

At low hydrogen pressures and low interaction temperatures, hydrogen absorption rates are low and hydrogenation proceeds via a formation of interstitial type $LaNi_3H_{3-5}$ hydrides. *In situ* SR XRD study of the 1st hydrogenation of $LaNi_3$ [14] performed at room temperature and 4.8 bar H_2 showed a two-step hydrogenation process yielding two crystalline hydrides, $LaNi_3H_3$ and $LaNi_3H_{4.6}$. The

Table 2
Crystal structure data for the $La_{3-x}Mg_xNi_9$ (*PuNi₃* type) intermetallic compounds from the Rietveld refinements of the SR XRD data (SNBL, BM01B, λ = 0.5009(1) Å). Space group $R\bar{3}m$ (no. 166).

Composition	$La_{2.51(2)}Mg_{0.49(2)}Ni_9$	$La_{2.30(4)}Mg_{0.70(4)}Ni_9$	$La_{2.00(2)}Mg_{1.00(2)}Ni_9$	$La_{1.47(1)}Mg_{1.53(1)}Ni_9$	$La_{1.09(1)}Mg_{1.91(1)}Ni_9$
La1 in 3*a* (0, 0, 0)					
$U_{iso} \times 100$ (Å²)	1.11(6)	0.9(1)	1.1(1)	0.82(4)	0.43(5)
La2/Mg in 6*c* (0, 0, *z*)					
z	0.14001(9)	0.1414(2)	0.1430(2)	0.1426(1)	0.1453(3)
$U_{iso} \times 100$ (Å²)	0.91(7)	0.9(2)	1.3(1)	1.0(1)	1.2(3)
n_{Mg},($n_{La} = 1 - n_{Mg}$)	0.244(9)	0.35(2)	0.50(1)	0.764(5)	0.954(5)
Ni1 in 3*b* (0, 0, 1/2)					
$U_{iso} \times 100$ (Å²)	1.20(7)	0.4(2)	0.2(1)	0.9(1)	0.7(1)
Ni2 in 6*c* (0, 0, *z*)					
z	0.3325(2)	0.3312(4)	0.3318(3)	0.3332(1)	0.3335(2)
$U_{iso} \times 100$ (Å²)	0.89(9)	0.9(2)	0.7(2)	0.55(6)	0.13(8)
Ni3 in 18*h* (*x*, −*x*, *z*)					
x	0.4988(4)	0.4993(8)	0.4994(6)	0.5007(2)	0.5009(3)
z	0.08174(7)	0.0823(2)	0.0831(2)	0.08455(5)	0.08529(8)
$U_{iso} \times 100$ (Å²)	0.71(5)	0.6(1)	0.67(9)	0.62(4)	0.57(5)
R-factors					
R_p	12.0	15.5	13.2	7.33	8.93
R_{wp}	15.6	19.9	17.4	9.56	11.9
χ^2	1.82	1.44	1.91	1.91	2.00

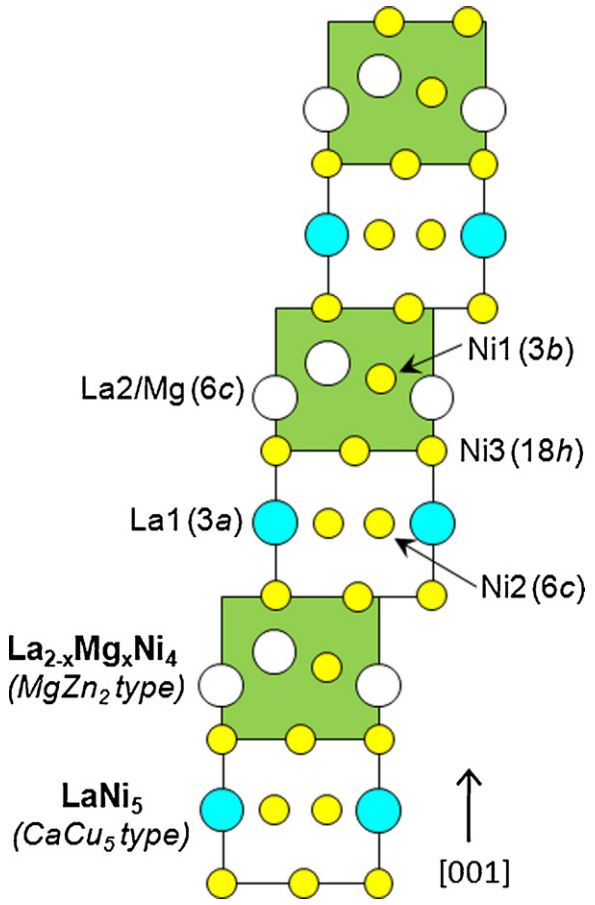

Fig. 3. Crystal structures of the $La_{3-x}Mg_xNi_9$ compounds (*PuNi*$_3$ type) shown as a stacking of the $LaNi_5$ (Haucke *CaCu*$_5$ type) and $La_{2-x}Mg_xNi_4$ (Laves *MgZn*$_2$ type) slabs along the trigonal [0 0 1] axis.

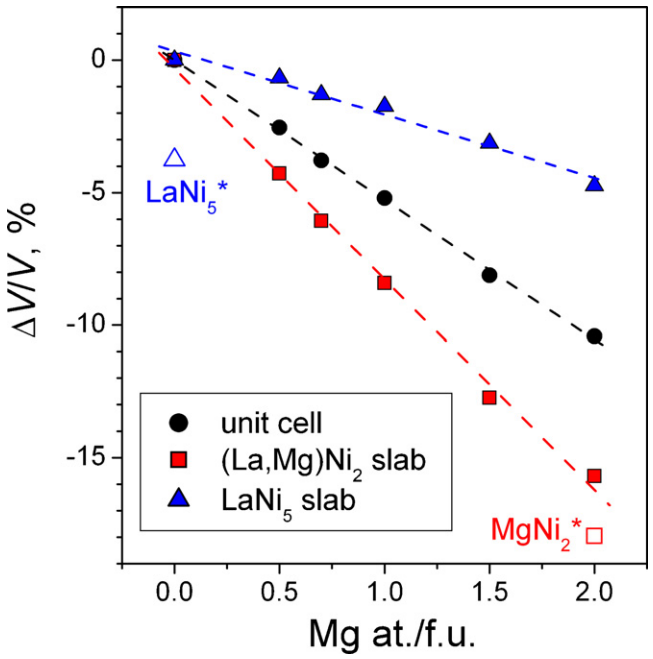

Fig. 4. Relative changes in the volumes of the unit cells and constituent fragments of the $La_{3-x}Mg_xNi_9$ structures during the Mg → La substitution. Relative volumes of the individual $LaNi_5$ and $MgNi_2$ compounds are given for comparison.

crystal structure of the monoclinic $LaNi_3D_3$ was solved earlier using the neutron powder diffraction data [15] and was found to be formed via anomalously large anisotropic expansion of the unit cell along [0 0 1] ($\Delta c/c = 30.6\%$). The basal plane was only slightly deformed on hydrogenation ($\Delta a/a$ contraction was 1.8–3.0%). The structure of the higher hydride, $LaNi_3H_{4.6}$, is presently unknown.

At higher hydrogen pressures and higher temperatures, $LaNi_3$ disproportionate during its interaction with hydrogen gas. It undergoes a hydrogen-induced amorphisation already during the first hydrogenation at room temperature [16], followed by a disproportionation on further H_2 absorption–desorption cycling at room temperature or when heated above 200 °C [17].

Interstitial $LaNi_3H_x$ hydrides are rather stable. It is not possible to desorb hydrogen from these hydrides at ambient temperature. However, during the heating in vacuum above 200 °C, the desorption takes place, during which the interstitial $LaNi_3H_{4.6}$ hydride decomposes into the amorphous products. Further heating of these amorphous products yields crystalline $LaNi_5$ and LaH_{3-x} [14]. During the thermal hydrogen desorption at 600 °C, LaH_2 decomposes and participates in the recombination process to reversibly form the initial $LaNi_3$ intermetallic alloy.

The $La_{2.5}Mg_{0.5}Ni_9$ compound with the lowest studied in the present work Mg content, forms poorly crystalline or amorphous hydrides, depending on the hydrogenation conditions. The formed hydrides are rather stable; their decomposition is not completed even in dynamic vacuum at ~100 °C (only 25% of the saturation H storage capacity can be released at 0.02 bar H_2 and 20 °C).

In situ SR XRD study showed that partially amorphous $La_{2.5}Mg_{0.5}Ni_9$-based hydride, in contrast to $LaNi_3H_{4.6}$, can completely recombine to form the initial $La_{2.5}Mg_{0.5}Ni_9$ alloy by its heating in vacuum to 450 °C, where a full hydrogen desorption and recrystallisation takes place. Thus, Mg substitution increases stability of the metal sublattice towards its disproportionation in hydrogen.

Amorphisation of the samples with higher Mg content ($x = 0.7$–2.0) is not observed during their hydrogenation; instead, the crystalline hydrides are formed. Thus, increase in Mg content increases the stability of the metal matrices against the hydrogen-induced amorphisation and results in a reversibility of the hydrogen absorption–desorption process. In the compositions range between La_2MgNi_9 and $LaMg_2Ni_9$, the hydrogenation becomes a completely reversible process, and a full cycle of hydrogen absorption and desorption giving reproducible values of the hydrogen storage capacities can be repeated many times.

Magnesium, when introduced into the $La_{3-x}Mg_xNi_9$ alloys, dramatically changes the hydrogenation behaviour. In the whole substitution range ($x = 0.0$–2.0) these alloys form hydrides $La_{3-x}Mg_xNi_9H_{9.2-13.9}$ containing 1.3–1.6 wt.% H (see Fig. 5). While hydrogen content in the saturated hydrides, *H*/*M*, slightly decreases with increase of the Mg/La ratio, H weight content for the same materials increases reaching its maximum of 1.58 wt.% H for the La_2MgNi_9-based hydride. The reversible H capacity is rather small at low Mg content (not shown in Fig. 5); it reaches the highest levels when 50% of La is substituted by Mg in the *MgZn*$_2$-type slabs.

Significant values of the hydrogen storage capacity of 1.3 wt.% H were measured even at the highest possible substitution level of La by Mg, in $LaMg_2Ni_9$, though high charging hydrogen pressures and low temperatures should be applied (Fig. 6). This is in disagreement with the previous research [4,7], possibly, because the experimental conditions used in the present work were not utilised in the earlier studies [4,7]. Importantly, observed values of H capacities cannot be explained by exclusive hydrogen insertion into the $LaNi_5$ slabs, and need H incorporation into the $MgNi_2$ fragments of the structure to reach the experimentally observed *H*/*M* ratios. This clearly shows an influence of the $LaNi_5$ layer in the hybrid structures on the hydrogenation of the $MgNi_2$ slabs, which

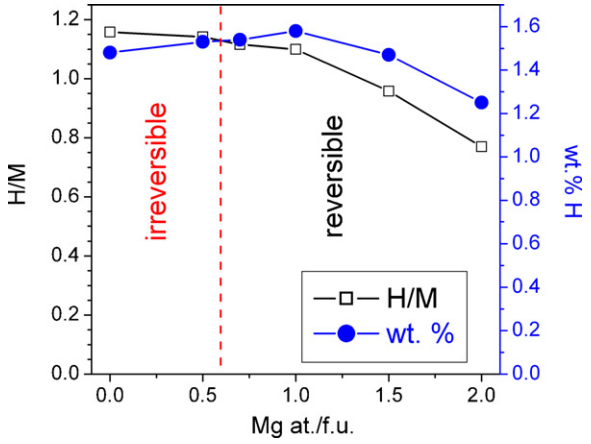

Fig. 5. Hydrogen content in the hydrides of the $La_{3-x}Mg_xNi_9$ compounds, saturated with hydrogen at room temperature and pressures 10–25 bar ($La_3Mg_0Ni_9$–$La_{1.5}Mg_{1.5}Ni_9$) and 244 bar ($LaMg_2Ni_9$).

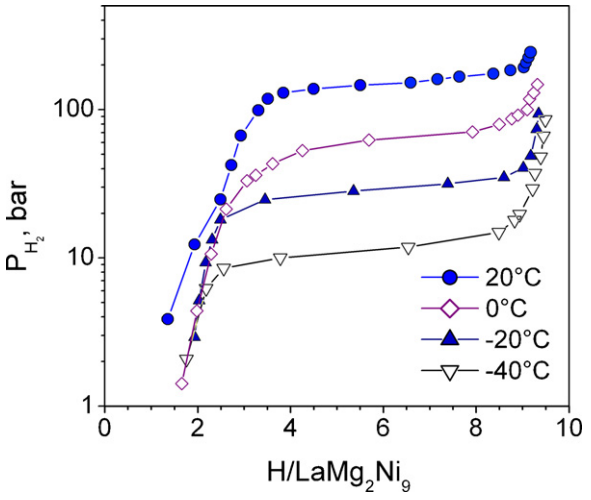

Fig. 6. Hydrogen absorption isotherms for the $LaMg_2Ni_9$ compound.

for the individual $MgNi_2$ compound was achieved only at a level of pressures of several kbar H_2 [18,19].

Isotherms of hydrogen absorption and desorption in the $La_{3-x}Mg_xNi_9$–H_2 systems at 20 °C are shown in Fig. 7. As can be seen from this figure, for Mg content 0.7–2.0 a fully reversible hydrogenation takes place with the single plateau equilibria observed in the isotherms between the hydrides and the alloys.

Thermodynamic parameters of hydride formation and decomposition calculated from the Van't Hoff plots (Fig. 8) are listed in Table 3. We note that the PCT-based thermodynamic data of the present study show a very significant variation of the values of the hydrogen equilibrium pressures versus the Mg content. These observed differences are much stronger as compared to the data of the earlier reported electrochemical charge–discharge isotherms [7].

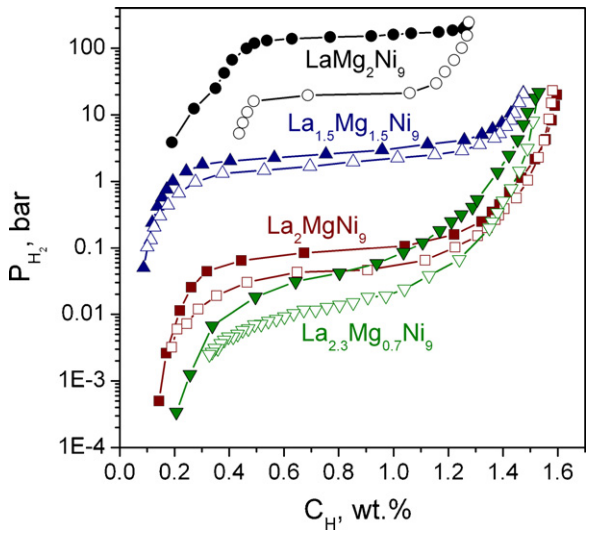

Fig. 7. Absorption–desorption isotherms in the $La_{3-x}Mg_xNi_9$–H_2 systems at 20 °C. Absorption: filled symbols; desorption: open symbols.

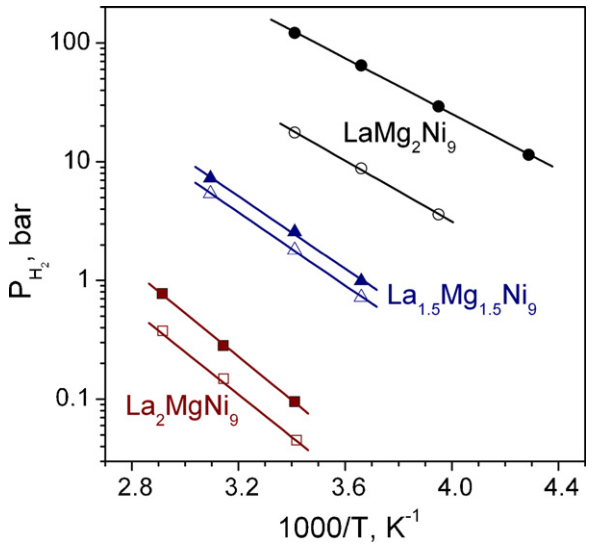

Fig. 8. Van't Hoff plots for the $La_{3-x}Mg_xNi_9$ hydrides. Absorption: filled symbols; desorption: open symbols.

Indeed, Fig. 7 shows a huge variation of the stabilities of the $La_{3-x}Mg_xNi_9$-based hydrides, reflected also by the corresponding large changes in the enthalpies of the hydride formation, from −24 to −40 kJ$(mol_{H_2})^{-1}$ (see also Table 3). Indeed, when Mg content increased from $x = 0.7$ in $La_{2.3}Mg_{0.7}Ni_9$ to 2 in $LaMg_2Ni_9$, equilibrium pressures of hydrogen desorption changed by a factor of more than 1000, from 0.011 bar H_2 to 18 bar H_2 at room temperature.

Interestingly, equilibrium absorption-desorption H_2 pressures (log scale) show an almost linear dependence from the Mg content (Fig. 9). As a linear dependence is also observed between the Mg content and the unit cell volumes of the $La_{3-x}Mg_xNi_9$ compounds,

Table 3
Thermodynamic parameters of the phase equilibria measured for the $La_{3-x}Mg_xNi_9$–H_2 systems.

Alloy	ΔH_{abs}, kJ$(mol_{H_2})^{-1}$	ΔS_{abs}, J$(mol_{H_2})^{-1}$	ΔH_{des}, kJ$(mol_{H_2})^{-1}$	ΔS_{des}, J$(mol_{H_2})^{-1}$	$P_{eq,abs}$ (20 °C), bar	$P_{eq,des}$ (20 °C), bar
$La_{2.3}Mg_{0.7}Ni_9$[a]	−37.4	–	40.3	–	0.036	0.011
$La_{2.0}Mg_{1.0}Ni_9$	−35.0 ± 0.8	−99.6 ± 2.5	35.9 ± 0.3	96.7 ± 0.9	0.095	0.045
$La_{1.5}Mg_{1.5}Ni_9$	−29.2 ± 1.2	−107.1 ± 4.2	29.5 ± 0.5	105.6 ± 1.6	2.5	1.8
$La_{1.0}Mg_{2.0}Ni_9$	−22.5 ± 0.3	−116.7 ± 1.2	24.0 ± 0.8	108.6 ± 2.8	122	18

[a] ΔH was calculated from the value of equilibrium H_2 pressure at 293 K, assuming that $\Delta S = 100$ J$(mol_{H_2}\ K)^{-1}$.

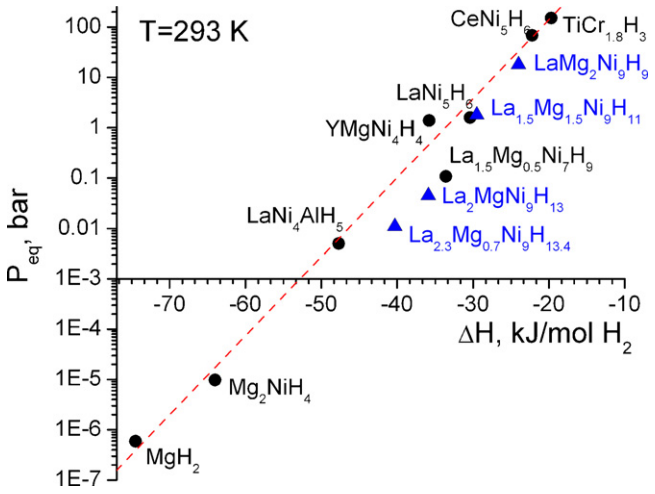

Fig. 9. Equilibrium desorption pressures P_{eq} versus heats of formation ΔH for the $La_{3-x}Mg_xNi_9$-based hydrides as compared to the reference hydrides.

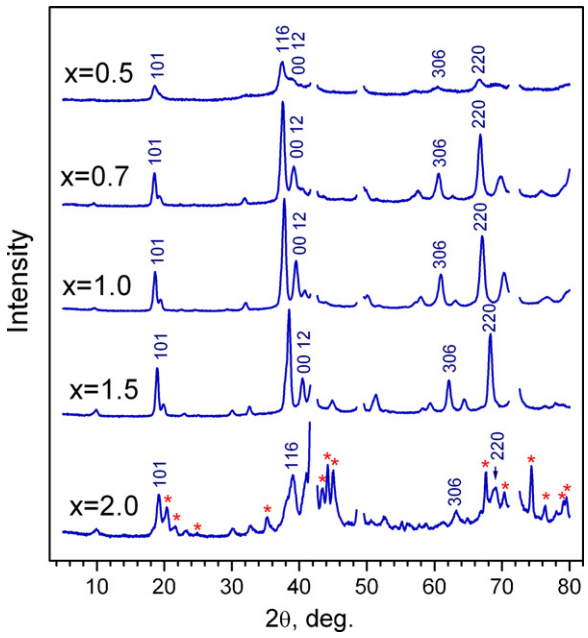

Fig. 10. *In situ* NPD pattern ($\lambda = 1.494$ Å; room temperature) of the $La_{3-x}Mg_xNi_9D_{9.5-13.5}$ deuterides. Miller indexes of the strongest peaks for the deuterides are shown. 2θ regions containing the peaks from the stainless steel sample cell are not shown for simplicity. In the $La_2MgNi_9D_{9.5}$ sample, a considerable amount of undeuterated La_2MgNi_9 (~40%; peaks marked by asterisks) is observed.

this means that for the chemically related alloys the stability of the hydrides is determined by a degree of the contraction/expansion of the unit cells of the intermetallic alloys. Not surprisingly, a similar correlation between the unit cell volumes and the stabilities of the hydrides/equilibrium hydrogen pressures was also observed for the substituted $LaNi_{5-x}M_x$ hydrides (M = Co, Al, Mn, Cu etc.) [20]. Thus, control over magnesium content by changing of the Mg/La ratio in the $La_{3-x}Mg_xNi_9$ compounds allows to achieve a large variation in the hydride thermal stabilities.

3.3. *In situ* diffraction studies of hydrogen absorption and desorption

Taking into account a complexity of the $La_{3-x}Mg_xNi_9$ structures, precise determination of the crystal structures of the hydrides requires a combined use of synchrotron X-ray and neutron powder diffraction. Such an approach was applied in present work, where we have used both these techniques applied under controlled pressure–temperature conditions.

Fig. 10 shows *in situ* neutron diffraction pattern of the $La_{3-x}Mg_xNi_9D_{9.5-13.5}$ deuterides collected for the samples with different Mg content ($x = 0.5, 0.7, 1.0, 1.5$ and 2.0) at room temperature and D_2 pressures in a range from 3.5 to 25 bar. A complete saturation of the alloys with deuterium gas was observed for the samples with lower magnesium content, for $x \leq 1.5$. In contrast, for $LaMg_2Ni_9$ even at the highest deuterium pressure applied of 25 bar D_2, deuteration was only partial, and a two-phase mixture of the alloy and corresponding deuteride was observed at a deuteration temperature of −30 °C (interaction time was ~20 h). Since temperature–pressure conditions were rather close to the equilibrium ones (see Fig. 6), the transformation was slow and was not completed on a time scale of the measurements performed.

Magnesium-containing $La_{3-x}Mg_xNi_9$ alloys, when Mg content surpasses a threshold of $x = 0.7$, show increased stability of the metal sublattice towards amorphisation. Well crystalline hydrides are formed; these hydrides retain initial trigonal symmetry of the unit cells. Lattice expansion appears to be nearly equivalent in all crystallographic directions, indicating formation of "isotropic" hydrides (see Table 4). However, at low Mg content (less than 0.7 Mg per formula unit) $La_{3-x}Mg_xNi_9$ alloys are still a subject for the amorphisation process, especially when cycling of hydrogen charge and discharge takes place.

In situ studies also show that the presence of magnesium in the alloys, even at its low content like in the $La_{2.5}Mg_{0.5}Ni_9$, allows an easy recombination the initial metal matrixes from the partially amorphous hydrides, by applying low temperature vacuum annealing (Fig. 11). This contrasts with the behaviour of the amorphised $LaNi_3$ hydride, which on vacuum heating instead of recombination disproportionates into $LaNi_5$ and LaH_2.

Liao et al., studied electrochemical hydrogenation of the alloys in a composition range from $La_{1.6}Mg_{1.4}Ni_9$ to $La_{2.2}Mg_{0.8}Ni_9$ [9] and found that these hydrides are formed via an *isotropic* expansion of the initial *PuNi*$_3$ type structure. An increase in La content leads to the corresponding increase in the volume expansion increment per absorbed hydrogen atom from 3.27 to 3.77 Å^3 per H atom. In contrast, present *in situ* studies do not show a dependence between ΔV/at.H and the La/Mg ratio, with ΔV/at.H values

Table 4
Crystallographic data for the $La_{3-x}Mg_xNi_9(H,D)_{9.5-13.5}$ (filled *PuNi*$_3$ type; sp.gr. $R\bar{3}m$; no. 166) hydrides/deuterides from the Rietveld refinements of the *in situ* SR XRD and NPD data.

Hydride/deuteride	*P*/*T* conditions	*a* (Å)	*c* (Å)	*V* (Å^3)	$\Delta a/a$ (%)	$\Delta c/c$ (%)	$\Delta V/V$ (%)	ΔV/at.H (Å^3)
$La_{2.5}Mg_{0.5}Ni_9D_{13.5}$	3.5 bar/27 °C	5.442(1)	26.89(1)	689.5(4)	7.5	9.0	25.9	3.78
$La_{2.3}Mg_{0.7}Ni_9D_{13.3}$	5.0 bar/27 °C	5.4356(2)	26.854(3)	687.12(7)	7.7	9.6	27.1	3.70
$La_2MgNi_9H_{13}$	9.6 bar/25 °C	5.4147(1)	26.607(1)	675.57(4)	7.6	9.5	26.8	3.66
$La_2MgNi_9D_{13.0}$	10.2 bar/27 °C	5.4151(2)	26.585(2)	675.12(6)	7.6	9.4	26.7	3.65
$La_{1.5}Mg_{1.5}Ni_9H_{11}$	22.8 bar/30 °C	5.3278(4)	25.890(3)	636.4(1)	6.9	7.8	23.2	3.64
$La_{1.5}Mg_{1.5}Ni_9D_{11.1}$	13.9 bar/27 °C	5.3307(1)	25.931(2)	638.14(5)	7.0	8.0	23.6	3.59
$LaMg_2Ni_9D_{9.5}$	25 bar/27 °C	5.263(1)	25.81(2)	619.2(4)	6.5	8.4	23.0	4.06

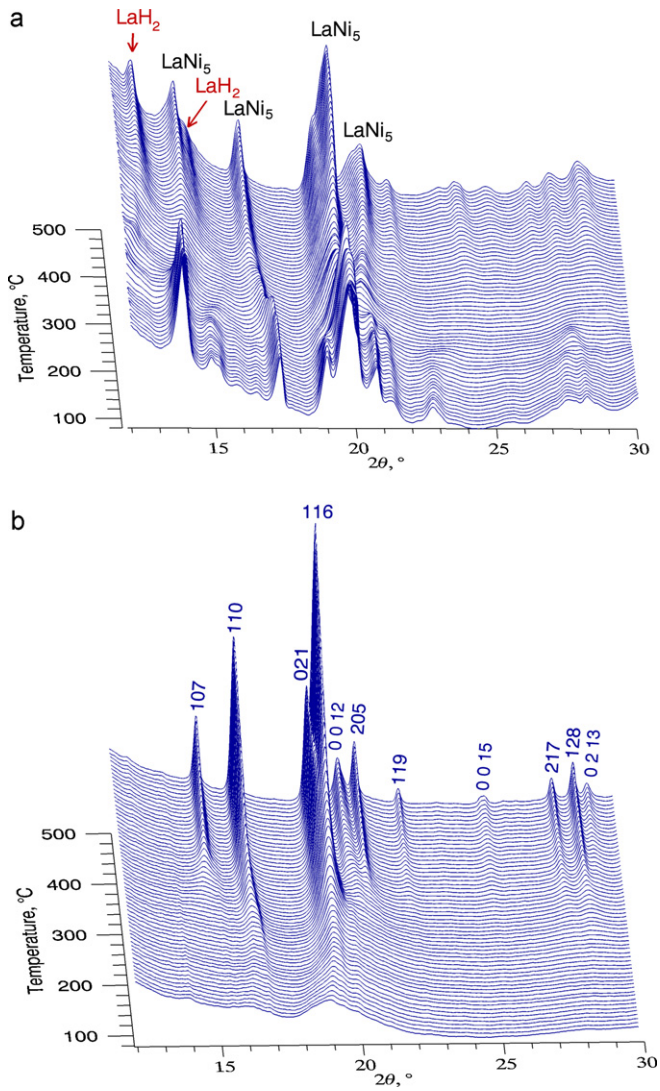

Fig. 11. Evolution of the *in situ* SR XRD pattern of the hydrides of $LaNi_3$ (a) and $La_{2.5}Mg_{0.5}Ni_9$ (b) compounds during their heating in dynamic vacuum (rate 5 °C/min) (SNBL, BM01A, λ = 0.7207 Å). $LaNi_3$ was hydrogenated at room temperature and 4.8 bar H_2 and formed a crystalline hydride, which during its heating in vacuum above 250 °C disproportionates into LaH_2 and $LaNi_5$. $La_{2.5}Mg_{0.5}Ni_9$ was hydrogenated at 90 °C and 11 bar H_2 and formed an amorphous hydride; during its heating in vacuum it recrystallises into the $La_{2.5}Mg_{0.5}Ni_9$ intermetallic (Miller indices of the peaks are given).

for the formation of the $La_{3-x}Mg_xNi_9(H,D)_{9.5-13.5}$ (x = 0.5–2.0) varying between 3.59 and 4.06 Å^3. Such a discrepancy apparently results from a partial decomposition of the hydrides during the *ex situ* XRD studies in [9], in contrast to the conditions of the *in situ* diffraction measurements used in present work. Not surprisingly, present *in situ* data yield noticeably larger unit cell parameters for the $La_2MgNi_9H_{13}$ hydride ($\Delta V/V$ = 26.7%) as compared to the data reported in [8,9] for the electrochemically saturated with hydrogen sample ($La_2MgNi_9H_{12.4}$; a = 5.3809, c = 26.5379 Å; V = 665.4 Å^3; $\Delta V/V$ = 24.8%).

Rietveld refinements of the PND data proved that both $LaNi_5$ (*CaCu*$_5$ type) and $La_{2-x}Mg_xNi_4$ (*MgZn*$_2$ type) layers are occupied by hydrogen atoms in the whole substitution range (x = 0.5–2.0).

We note that the volumes of the slabs in the hydrides change similarly to the initial compounds. The volumes of both the *CaCu*$_5$ and *MgZn*$_2$ slabs in the structures of the hydrides decrease upon increasing the Mg content; $V_{La_{2-x}Mg_xNi_4}$ changes from 116 Å^3 (x = 0.5) to 95 Å^3 (x = 2.0) for the Laves-type slabs. For the *CaCu*$_5$ slabs a less significant yet substantial contraction takes place, when V_{LaNi_5} decreases from 114 to 110 Å^3. Relative volume changes $\Delta V/V$, also reflect modifications in the Mg content. Expansion of the $LaNi_5$ slab varies from 26 to 30% (a minimum value is for $La_2MgNi_9H_{13}$ and maximum expansion is for $LaMg_2Ni_9H_9$). Hydrogen-induced expansion of the $La_{2-x}Mg_xNi_4$ slabs changes in the range 16–27% with maximum for the $La_2MgNi_9H_{13}$ and minimum for the $LaMg_2Ni_9H_9$. Significant volume expansion of the $MgNi_2$ slab, 16%, in $LaMg_2Ni_9H_9$ is a prominent feature of the effect of the neighbouring $LaNi_5$ slabs on a cooperative hydrogenation of the $MgNi_2$ slab and obviously proves that this slab accommodates H atoms.

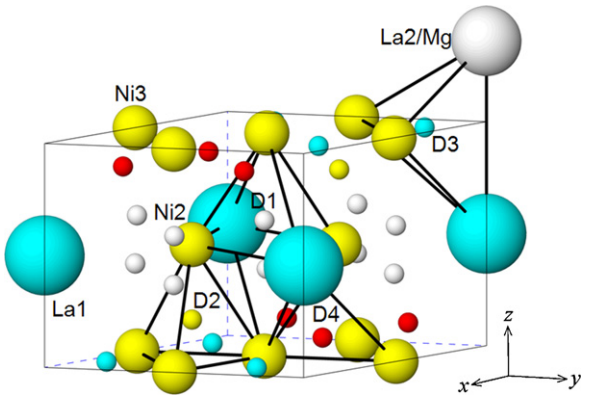

Fig. 12. Hydrogen distribution in the *CaCu*$_5$-type slab of the crystal structures of the $La_{3-x}Mg_xNi_9D_{9.5-13.5}$. Four types of D atoms are shown: D_1 in [La_2Ni_4] octahedron; D_2 in [Ni_4] tetrahedron; D_3 and D_4 in [$(La,Mg)_2Ni_2$] tetrahedra.

From the refinements of the NPD data it was found that the overall chemical composition $LaMg_2Ni_9H_{9.5}$ then can be presented as $LaNi_5H_{5.7} + 2 \times MgNi_2H_{1.9}$. Thus, in the hybrid $LaMg_2Ni_9$ structure, $LaNi_5$-assisted hydrogenation of the $MgNi_2$ slab proceeds at rather mild H_2/D_2 pressure conditions; the equilibrium D_2 desorption pressure is just 20 bar D_2. In contrast, individual $MgNi_2$ intermetallic remains inert with respect to the hydrogenation even at much higher hydrogen pressures. The refinements showed a partial filling by D atoms of the four types of the tetrahedral interstices in the $MgNi_2$ slab; these include two types of the available [$MgNi_3$] (18*h* and 6*c*) and two types of the [Mg_2Ni_2] (36*i* and 18*h*) interstitial sites.

In addition, similar to the other studied $La_{3-x}Mg_xNi_9$-based deuterides, the remaining 5.7 at. D/f.u. form a standard hydrogen sublattice within the $LaNi_5$ slab and are statistically distributed in the four types of the interstices; hydrogen atoms partially occupy [La_2Ni_4] octahedra and three types of tetrahedra, [Ni_4] and two types of the [$LaMgNi_2$] sites.

A more detailed crystallographic analysis of the deuterium sublattice in the structures of $La_{3-x}Mg_xNi_9(H,D)_{9.5-13.5}$ will be presented in a forthcoming publication [21]. In the present work we would like to limit the discussions of our findings to some most general structural features.

Deuterium sublattice of the $La_{3-x}Mg_xNi_9(H,D)_{9.5-13.5}$ deuterides is disordered with a partial and statistical occupation of the interstices taking place in both *CaCu*$_5$ and *MgZn*$_2$ type structure parts.

The distribution of H atoms in the $LaNi_5$ slabs appears to be quite similar for the whole Mg → La substitution range. In these slabs D atoms fill three types of interstitial sites: deformed octahedron [La_2Ni_4], and tetrahedra [Ni_4] and [$(La,Mg)_2Ni_2$] (see Fig. 12). D distribution resembles the crystal structure of the saturated deuterides of the individual $LaNi_5$ compound [22–24]. As example, in the $La_{1.5}Mg_{1.5}Ni_9D_{11}$ deuteride the overall stoichiometry can be presented as $LaNi_5D_{6.8} + La_{0.5}Mg_{1.5}Ni_4D_{4.3}$. In the $LaNi_5D_{6.8}$ slab of the $La_{1.5}Mg_{1.5}Ni_9D_{11}$, the D atoms are distributed as: 2.48 D in

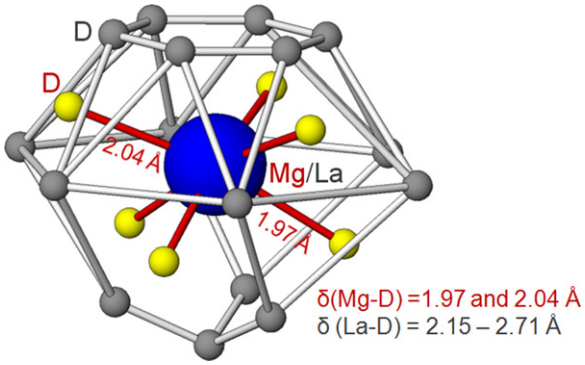

Fig. 13. D sublattice inside the $LaMgNi_4$ slab of the structure of the $La_2MgNi_9D_{13}$ deuteride. The central position is occupied by La or Mg. D sites form two different coordination spheres: an internal deformed octahedron centered by Mg (at much shorter distances of 1.97–2.04 Å) and an external 16-vertex polyhedron centered by La (with significantly longer La–D separations of 2.15–2.71 Å).

$[La_2Ni_4]$, 0.75 D in $[Ni_4]$ and 3.59 D in $[(La,Mg)_2Ni_2]$. This completely resembles the structure of the individual hydrides $LaNi_5D_{6.5}$ (2.68 D in $[La_2Ni_4]$, 0.78 D in $[Ni_4]$ and 3.1 D in $[La_2Ni_2]$) [24] and $LaNi_5D_{6.7}$ (3 D in $[La_2Ni_4]$, 0.83 D in $[Ni_4]$ and 2.87 D in $[La_2Ni_2]$) [22].

In contrast, distribution and coordination of the D atoms inside the $La_{2-x}Mg_xNi_4$ slabs strongly depends on the x value. Occupancy of these slabs gradually decreases with increasing the Mg content. This is accompanied by a significant modification of the hydrogen sublattice, where types of the filled by hydrogen interstitial sites vary for the different compounds with changing Mg content [21].

An interesting and rather unexpected distribution of D atoms is observed in the structure of $La_2MgNi_9D_{13}$. In this structure the composition of the $MgZn_2$ type slab is $LaMgNi_4$, with equal statistical occupancy of the 6*c* site by La and Mg atoms. D atoms statistically occupy four types of the interstices, including tetrahedra $[(La,Mg)_2Ni_2]$, $[(La,Mg)Ni_3]$ and $[Ni_4]$, and trigonal bipyramids $[(La,Mg)_3Ni_2]$.

From analysis of the distances between La/Mg atoms and deuterium atoms, we deduce a 16-fold coordination of La by D (at distances between 2.15 and 2.71 Å) and an octahedral coordination of Mg which locally leads to the formation of MgH_6 (here much shorter distances Me–D are observed, 1.97 and 2.04 Å), as shown in Fig. 13. The same type of the local D sublattice was observed in the $LaMgNi_4$ slab of the structurally related $La_{1.5}Mg_{0.5}Ni_7D_{9.1}$ deuteride (filled Ce_2Ni_7 type) [25]. Octahedral MgD_6 configuration appears to be typical for the Mg-containing hydrides; an example is magnesium hydride, where both α- and γ-MgH_2 hydrides [26] contain the MgH_6 octahedra. Not surprisingly, the interatomic distances Mg-D in the structures of $La_2MgNi_9D_{13}$ and $La_{1.5}Mg_{0.5}Ni_7D_{9.1}$ are close to those in the structures of MgH_2 (1.92–2.00 Å). This fact implies a possible formation of the local Mg-D bonding in the $La_{3-x}Mg_xNi_9(H,D)_{9-13.5}$ deuterides. The other interesting example of the formation of the MgD_6 coordination is the structure of the γ-deuteride of the $LaMgNi_4$ compound ($MgCu_4Sn$ type, ordered derivative of the Laves $MgCu_2$ type) studied by Chotard et al. [27]. In the cubic γ-$LaMgNi_4D_{4.58}$ deuteride it was observed nearly a complete filling of the two types of the D sites: D_1 occupies a bipyramid $[La_2MgNi_2]$ and D_2 is in the tetrahedral $[Ni_4]$ interstice [27]. Analysis of the structure of γ-$LaMgNi_4D_{4.58}$ shows that D atoms form a regular octahedron around the Mg atoms (with Mg-D distances of 2.01 Å) and a tetrahedron around the Ni atoms. D sublattice can be presented as an ordered spatial framework of MgD_6 and NiD_4.

4. Conclusions

Magnesium dramatically affects the hydrogenation–dehydrogenation behaviours of the ternary $La_{3-x}Mg_xNi_9$ *$PuNi_3$* type alloys allowing a fine tuning of the stabilities of the formed hydrides and optimisation of their behaviours relevant for different applications. These alloys were synthesised using the developed powder metallurgy routes yielding nanostructured materials with controlled Mg content, thus overcoming difficulties of Mg loss during the melting process.

Mg influences structural features of the hydrogenation process and determines various aspects of hydrogen interaction with the $La_{3-x}Mg_xNi_9$ intermetallics causing:

- Substantial decrease of the thermodynamic stability of the hydrides with equilibrium hydrogen desorption pressures changing by a factor of 1000, from 0.01 bar to 20 bar H_2, by modifying the Mg content.
- Improvement of the stability of the alloys during cycling of hydrogen charge and discharge and their resistance against the hydrogen-induced amorphisation and disproportionation.
- Increase of the reversible hydrogen storage capacity following increase of x in the $La_{3-x}Mg_xNi_9$ with its highest value reached when 50% of La in the *$MgZn_2$*-type slabs was substituted by Mg to form the La_2MgNi_9 alloy.
- Change of the mechanism of the formation of the hydride crystal structures during the hydrogenation from *anisotropic* to *isotropic* one.

Established composition–structure–properties relationships in the ternary $La_{3-x}Mg_xNi_9$ intermetallics will allow a better selection of the optimised alloys in further development of the Ni-MH battery electrode materials with improved electrochemical performance.

Acknowledgements

This work received a support from the Norwegian Research Council. A skilful assistance from the staff of the Swiss-Norwegian Beam Lines during the experimental studies at ESRF is gratefully acknowledged. Dr. Jim Webb (Griffith University, Australia) and Dr. Denis Sheptyakov (PSI, Switzerland) are sincerely thanked for the collaboration in the neutron powder diffraction experiments.

References

[1] T. Kohno, H. Yoshida, F. Kawashima, T. Inaba, I. Sakai, M. Yamamoto, M. Kanda, J. Alloys Compd. 311 (2) (2000) L5–L7.
[2] K. Kadir, T. Sakai, I. Uehara, J. Alloys Compd. 257 (1997) 115–121.
[3] K. Kadir, H. Yamamoto, T. Sakai, I. Uehara, N. Kanehisa, Y. Kai, L. Eriksson, Acta Crystallogr. C 55 (1999), doi:10.1107/S0108270199098418, CIF access code: IUC 9900152.
[4] K. Kadir, T. Sakai, I. Uehara, J. Alloys Compd. 302 (2000) 112–117.
[5] J.J. Reilly Jr., R.H. Wiswall Jr., Inorg. Chem. 7 (11) (1968) 2254–2256.
[6] J. Chen, H.T. Takeshita, H. Tanaka, N. Kuriyama, T. Sakai, I. Uehara, M. Haruta, J. Alloys Compd. 302 (2000) 304–313.
[7] B. Liao, Y.Q. Lei, G.L. Lu, L.X. Chen, H.G. Pan, Q.D. Wang, J. Alloys Compd. 356–357 (2003) 746–749.
[8] B. Liao, Y.Q. Lei, L.X. Chen, G.L. Lu, H.G. Pan, Q.D. Wang, J. Alloys Compd. 376 (2004) 186–195.
[9] B. Liao, Y.Q. Lei, L.X. Chen, G.L. Lu, H.G. Pan, Q.D. Wang, J. Power Sources 129 (2004) 358–367.
[10] S. De Negri, M. Giovannini, A. Saccone, J. Alloys Compd. 439 (2007) 109–113.
[11] J. Rodriguez-Carvajal, Newsletter 26 (2001) 12–19.
[12] A.V. Virkar, A. Raman, J. Less-Comm. Met. 18 (1969) 59–66.
[13] J.-F. Berar, P. Lelann, J. Appl. Crystallogr. 24 (1991) 1–5.
[14] R.V. Denys, A.B. Riabov, V.A. Yartys, J. Solid State Chem, to be submitted.
[15] R.V. Denys, A.B. Riabov, V.A. Yartys, R.G. Delaplane, M. Sato, J. Alloys Compd. 446–447 (2007) 166–172.
[16] H. Oesterreicher, J. Clinton, H. Bittner, Mat. Res. Bull. 11 (1976) 1241–1248.
[17] J. Zhang, G. Zhou, G. Chen, M. Latroche, A. Percheron-Guégan, D. Sun, Acta Mater. 56 (2008) 5388–5394.

[18] R. Kataoka, Y. Goto, A. Kamegawa, H. Takamura, M. Okada, Mater. Trans. 47 (8) (2006) 1957–1960.
[19] R. Kataoka, Y. Goto, A. Kamegawa, H. Takamura, M. Okada, J. Alloys Compd. 446–447 (2007) 142–146.
[20] A. Percheron-Guégan, C. Lartigue, J.C. Achard, J. Less-Comm. Met. 109 (1985) 287–309.
[21] R.V. Denys, V.A. Yartys, C.J. Webb, D. Sheptyakov, J. Phys. Chem. C, to be submitted.
[22] C. Lartigue, A. Percheron-Guégan, J.C. Achard, J.L. Soubeyroux, J. Less-Comm. Met. 113 (1985) 127–148.
[23] P. Thompson, J.J. Reilly, L.M. Corliss, J.M. Hastings, R. Hempelmann, J. Phys. F: Met. Phys. 16 (1986) 675–685.
[24] M. Latroche, J.-M. Joubert, A. Percheron-Gueégan, F. Bourée-Vigneron, J. Solid State Chem. 177 (2004) 1219–1229.
[25] R.V. Denys, A.B. Riabov, V.A. Yartys, M. Sato, R.G. Delaplane, J. Solid State Chem. 181 (2008) 812–821.
[26] M. Bortz, B. Bertheville, G. Böttger, K. Yvon, J. Alloys Compd. 287 (1999) L4–L6.
[27] J.-N. Chotard, D. Sheptyakov, K. Yvon, Z. Kristallogr. 223 (2008) 690–696.